EUROPEAN FUSION DEVELOPMENT AGREEMENT

EFDA–JET–PR(04)37

M. Endler, I. García-Cortés, C. Hidalgo, G.F. Matthews, ASDEX Team
and JET EFDA contributors

The Fine Structure of ELMs in the Scrape-Off Layer

The Fine Structure of ELMs in the Scrape-Off Layer

M. Endler[1], I. García-Cortés[2], C. Hidalgo[2], G.F. Matthews[3], ASDEX Team[1, 4] and JET EFDA contributors*

[1]Max-Planck-Institut für Plasmaphysik, EURATOM Association, D-17491 Greifswald
[2]Asociación EURATOM-CIEMAT, Madrid, Spain
[3]EURATOM/UKAEA Fusion Association, Culham Science Centre, Abingdon, Oxon. OX14 3DB, UK
[4]Max-Planck-Institut für Plasmaphysik, EURATOM Association, D-85748 Garching
** See annex of J. Pamela et al, "Overview of Recent JET Results and Future Perspectives", Fusion Energy 2000 (Proc. 18th Int. Conf. Sorrento, 2000), IAEA, Vienna (2001).*

Preprint of Paper to be submitted for publication in
Plasma Physics and Controlled Fusion

ABSTRACT

ELMs have been observed by diagnostic systems with high spatial and temporal resolution in the ASDEX and JET tokamaks. During the ELMs, substructures exist in the scrape-off layer with sizes of 2-5cm and lifetimes in the order of 20-50μs. Their poloidal-temporal evolution is directly observed, and the radial transport due to turbulent E×B drift in these substructures is estimated. A comparison is made between "normal" fluctuations in between ELMs and these substructures in terms of poloidal size and velocity and related radial transport. The increased radial transport during ELMs is shown to be mainly due to these substructures. The observed uctuation amplitudes and velocities of the substructures are found to be compatible with the model of radial transport by plasma "blobs" and plasma potential gradients generated by the sheath boundary conditions. The transport due to turbulent radial E×B flows is compared during and in between ELMs, and the observation of ELM substructures in the main plasma scrape-off layer is put into context with the observation of substructures on the target plates.

1. INTRODUCTION

Since the discovery of the state of improved con nement called H-mode in the ASDEX tokamak [1, 2], many investigations of the phenomenon called ELMs (edge-localised modes) have been conducted (for an overview, see [3, 4, 5]). ELMs are an instability associated with a rapid loss of particles and energy from the edge plasma onto the target plates and possibly the wall of the device. It was soon realised that a high temporal resolution in the μs range is necessary to resolve the fast changes during an ELM, which are observed, e. g., by Mirnov coils or reflectometry. Until recently, however, hardly any investigation existed of the spatial ne structure (on the scale of a few millimetres) of ELMs. It was then noted that a temporal substructure exists in the ion saturation current (I_{sat}) signals of Langmuir probes during ELMs in the main plasma Scrape-Off Layer (SOL) of the JET and MAST tokamaks, i. e., in the signals of spatially highly localised measurements [6, 7, 8, 9]. The same was noted in a comparative analysis of I_{sat}, electron temperature (T_e) and floating potential (Φ_{fl}) fluctuations during L-mode, ELMfree H-mode and during ELMs in DIII-D, where also the turbulent radial E×B particle and energy transport was investigated [10]. T_e fluctuations were also taken into account in a recent analysis of particle and electron energy transport during ELMs to the JET main chamber wall [11]. In measurements with multiple Langmuir probes with 0.5-1cm separation it could be demonstrated, that the temporal ELM substructures are indeed related to spatial substructures on the scale of 1-2cm [8, 9]. Such spatial substructures are also visible in poloidally resolved H_α emission measurements in the "old" ASDEX [9]. The analysis of JET Langmuir probe measurements was then extended to the calculation of the radial E×B velocity during ELMs [8, 9], and to a detailed statistical analysis of the relation between local radial gradients, radial and poloidal electric fields and effective radial transport velocity during ELMs [12]. It was soon realised that the spatial structures observed in the SOL during ELMs resemble the fluctuation "events" or "blobs" suggested by Krasheninnikov et al. to explain the radial particle transport in the

SOL due to "ordinary" fluctuations [13, 14], and the observed properties of the ELM substructures or "plasmoids" were compared with the predictions of this model ([10, 9] and, in detail, on a broad statistical basis and extending the model to the case of hot ions, [15]). Recently, toroidally non-symmetric substructures in the divertor plate power load were found 5-10cm outside the strike line during type I ELMs in ASDEX Upgrade with a fast infrared camera [16], and the lamentary structure of an ELM in the D_α light was made visible with a fast camera on MAST [17].

In this paper, we report on measurements during ELMs with a dedicated H_α/D_α fluctuation diagnostic system in the edge and SOL of the "old" ASDEX and with Langmuir probes in the SOL of JET. After a description of the diagnostic systems in section 2, we shall present the results of the ASDEX H_α measurements, where the poloidal size and propagation velocity of the ELM substructures is directly visible in addition to the temporal substructure (together with a comparison with divertor signals) in section 3. In section 4, we shall estimate the radial E×B transport from the JET Langmuir probe measurements and compare the transport during and in between type I ELMs. We shall then in section 5 briefly recall the mechansims generating electric potential gradients in the SOL, including the radial propagation mechanism in the model of SOL fluctuations as high-pressure "blobs" in a low-pressure background plasma, which was introduced in [13, 14]. In our discussion in section 6, we shall use these models to estimate propagation velocities for ELM substructures and "normal" fluctuations and compare them with the observations in order to nd a unified picture of ELM substructures and "normal" fluctuations. In addition, we shall compare the measured increase in radial transport with the values from transport modelling. Our conclusions will be presented in section 7.

2. DIAGNOSTIC SYSTEMS USED FOR ELM OBSERVATION

2.1. H_α/D_α DIAGNOSTICS IN ASDEX

In the midplane of ASDEX, an H_α/D_α Fluctuation Diagnostic (HFD) was used, which allowed to record the H_α/D_α radiation from the plasma edge with photomultipliers at 16 positions, which were spaced poloidally in steps of 6mm [18]. In order to increase the light intensity and to obtain a well-defined and constant in flux of neutral gas, hydrogen or deuterium was puffed through a gas valve into the observed edge region. EIRENE calculations showed that for the typical plasma parameters in the edge of fusion experiments, the H_α radiation originates mostly from a narrow radial layer of 1-2cm width centred slightly outside the Last Closed Magnetic Surface (LCMS).

For the plasma temperatures found in this region, the effective rate coefficient for the emission of H_α/D_α photons is only a weak function of plasma temperature, and the emission is proportional to the product of neutral gas density and electron density. In contrast to the common belief that the H_α intensity is a direct measure for the neutral gas influx only and is independent of the electron density, which is true in the stationary case, it has been shown that for electron densities fluctuating sufficiently fast, corresponding fluctuations of the H_α radiation do ensue, and its fluctuations are proportional to the local electron density, which was confirmed by comparison of fluctuation

measurements between the HFD and Langmuir probe and collective scattering measurements [19, 18].

In addition to the HFD, we use data from a photodiode observing the upper outer divertor plate with low spatial resolution. This "FDKO" signal was one of the standard monitor signals for LH-transitions and ELMs on ASDEX. The arrangement of both detector systems is shown in Fig. 1.

2.2. LANGMUIR PROBES IN JET

In the JET tokamak, a Reciprocating Langmuir Probe (RLP) system at the top of the plasma [20] was used for ELM investigations. It was fitted with a head comprising six carbon tips of 1.5mm diameter, arranged in two triples with 4.1 and 2.3mm poloidal separation between the tip centres within each triple, measuring Φ_{fl} fluctuations with the two outer tips and I_{sat} fluctuations with the central tip (see Fig.2). The three tips of each triple were placed on the same flux surface, and the centres of the triples were separated by 1.3cm in radial and 2.3cm in poloidal direction [21, 22]. The probe head was inserted into the edge plasma at the top of the machine with a vertical velocity below 0.6m/s, corresponding to 0.45m/s in minor radius or 0.3m/s in midplane minor radius. The arrangement of the RLP system on JET is shown in Fig. 3. The signals of the probes were digitised at a rate of 250kHz.

The arrangement on the RLP system of two poloidally displaced Langmuir probe tips measuring $\tilde{\Phi}_{fl}$ and a third tip in between measuring $\tilde{I}_{sat}$ can be used to calculate the fluctuation-induced radial E×B transport, if the probe tips are close enough to each other to allow a reliable calculation of the poloidal gradient of Φ_{fl} at the position of the intermediate probe tip, and if one neglects the effect of temperature fluctuations on the quantities $\tilde{\Phi}_{fl}$ and $\tilde{I}_{sat}$. Even if electron temperature fluctuations exist, their influence on the result is minimised, if they are in phase with the plasma density fluctuations [23].

3. SPATIAL NE STRUCTURE OF ELMS IN H_α /D_α LIGHT IN ASDEX

3.1. MIDPLANE

The H_α /D_α fluctuation diagnostic described in section 2.1 was used to investigate the spatio-temporal properties of the "normal" density fluctuations in the SOL of ASDEX[18]. In Fig. 4, an example for this "normal" turbulence, which is always present, is given. The fluctuations can be characterised by certain parameters like amplitude, spatial and temporal scales and poloidal velocity. These parameters vary for different discharge conditions. Note in particular that the poloidal velocity of the structures, as visible from their inclination in the poloidal-temporal representation of the raw data in Fig.4, is rather constant for stationary discharge conditions - in the case depicted here, a poloidal velocity of (1100 ± 300) m/s can be calculated from the inclination of the structures. In contrast, each ELM displays a different spatio-temporal structure when viewed with the same resolution as the "normal" fluctuations, which is demonstrated by three examples in Fig. 5. The spatial scale of the substructures seems to be comparable to that of "normal" fluctuations. However, the poloidal velocity of the substructures is in general much higher during ELMs and exhibits a

much larger scatter; often even structures with opposite poloidal velocity occur during one single ELM. In our examples, poloidal velocities between 14000m/s and +7500m/s occur ("+" denoting the ion diamagnetic drift direction, which is, due to the radial electric field and the resulting dominating E×B drift, the usual direction of propagation for the SOL fluctuations, see section 5). Due to the high poloidal velocity of these substructures, it is diffcult to give values for their lifetime, since the baselength of the array of observation is insufficient to follow them for a sufficiently long time. Only a lower estimate of 10-20μs can be given.

3.2. COMPARISON WITH DIVERTOR SIGNALS

Why have the strong and very short peaks in H_α/D_α intensity not been remarked in one of those H_α/D_α signals often used as monitors for ELM activity? For comparison, we display in Fig.6 several ELMs recorded by the HFD together with the "FDKO" signal, an H_α/D_α monitor signal from a photodiode observing the upper outer divertor plate with low spatial resolution (see section 2.1 and Fig.1). An averaging over 8 channels of the HFD, corresponding to a poloidal average over 9cm (displayed in blue), does hardly reduce the strong peaks and carries still much more similarity to the signal of one single channel (displayed in black) than to the FDKO signal (displayed in red). The fast initial rise of the FDKO intensity demonstrates that this diagnostic should be able to resolve peaks of 10-20μs duration. The principal difference between the two positions of observation is that the neutral gas in the divertor is exclusively due to recycling. During an ELM, the plasma flux onto the target plates and hence the neutral gas density increase strongly, whereas the neutral gas density in the observation region of the HFD is dominated by the constant gas puffing and stays almost constant. This can also explain why the peak intensity of the FDKO signal during an ELM is higher by a factor of 3-6 than in between ELMs in these examples, whereas the increase during the sharp peaks in the HFD signals is only by a factor 1.3-2. The substructure on top of the FDKO ELM signals, with an amplitude of only 15-30% of the total ELM amplitude and a time scale of 50-100μs, could then be due to peaks like those dominating the signal of the HFD.

3.3. WITH/WITHOUT GAS PUFFING

In a similar manner as in the divertor H_α/D_α signals, the fast substructures of an ELM are hardly visible in the HFD signals if we do not puff gas into the observed region. In this case, the light intensity from the observed region of the main chamber SOL decays back to its inter-ELM level even slower than the FDKO signal (see Fig. 7). As in the divertor, the increase in light intensity may now be dominated by increased recycling from the main chamber walls rather than by changes in the electron density. In addition, the light may originate in part from the torus inboard side, where the HFD is out of focus and cannot resolve spatio-temporal fine structures anyway.

4. LANGMUIR PROBE MEASUREMENTS OF ELMS AND RELATED E×B TRANSPORT IN JET

4.1. SPATIAL FINE STRUCTURE IN THE SOL OF THE MAIN PLASMA

During many ELMs, the tips of the RLP system described in section 2.2 started to emit due to the high heat loads. A full analysis of the data from these probes was therefore only possible for a small number of ELMs, especially for ELMs with smaller amplitude, for probe positions farther out in the SOL, and for the outermost rather than the innermost triple of probe tips.

The results of the RLP system for one such ELM are displayed in Fig. 8. Like in the HFD signals from the main chamber of ASDEX, strong peaks in the Isat signals occur with a duration of 10-50μs. When comparing the signals on the two I_{sat} tips, which are separated by 2.7cm perpendicular to the magnetic field, most strong peaks can be identified in both signals, however, their amplitude and the time lag between the two tips varies (even for substructures within the same ELM): It is not always the innermost tip (the one closer to the separatrix) which detects the higher amplitude or on which a peak occurs first. This indicates a spatial structure perpendicular to the magnetic field on a scale smaller than the probe tip separation of 2.7cm. (For limiter probes with a larger radial separation of several centimetres, a statistical delay of the ELM signal on the probes farther out in the limiter shadow with respect to the probes closer to the limiter edge was found and used to determine a radial propagation velocity of the substructures [15, Fig. 12].)

4.2. RADIAL E×B TRANSPORT DURING ELMS

The arrangement of the probe tip triples on the RLP system measuring Φ_{fl} and I_{sat} fluctuations allows to calculate the fluctuation-induced radial transport due to fluctuating radial E×B drifts (see section 2.2). As the neglect of temperature fluctuations in the case of ELMs may appear to be a very bold assumption, we shall interpret the results of our analysis only as a rough estimate of the true radial E×B transport during an ELM.

In the three lower panels of Fig. 8, the fluctuating radial E×B velocity $\tilde{v}_r$, the fluctuating radial particle flux $\tilde{\Gamma}_r$ and the integrated radial E×B particle flux are depicted. The latter two quantities are only known up to a factor $\sqrt{T_i + T_e}$ from the transformation of I_{sat} into plasma density - here, we assume an average temperature of 10eV.[1] Whereas the traces of $\tilde{v}_r$ and $\tilde{\Gamma}_r$ only display strongly increased fluctuation amplitudes, the trace of $\int\tilde{\Gamma}_r dt$ demonstrates that the net radial flux is indeed directed outwards, and the distinct steps show that the dominating contributions to this transport happen during those very brief intervals of 10-50μs, which are marked by the peaks in the I_{sat} signals. The radial E×B velocity during these intervals can reach 1000-2000m/s, with the largest amplitudes at the beginning of the ELM and the $\tilde{v}_r$ amplitude then decaying to its inter ELM value, as noted in [11]. Since we cannot follow individual peaks longer than they are registered on a single

[1]The value of 10eV was extrapolated from inter-ELM target plate profiles and converted to the upstream position of the RLP at the middle position during its reciprocation. There exist strong hints that T_i can exceed T_e by factors of up to 5-10 in JET H-modes, in particular in a narrow layer outside the separatrix [24]. This must be kept in mind when trying to draw conclusions based on the absolute values of Γ_r calculated in this article.

probe tip, the duration of 10-50μs is a lower estimate of their lifetime, and together with the radial E×B velocity we obtain a lower estimate of 1-10cm for the radial movement of plasma within these structures. From Fig. 8(d) it is evident, that, locally, the radial transport in an ELM occurs mainly concentrated within few (typically 1-3) short intervals of 10-50μs, coinciding with the strong peaks in the I_{sat} signals.

A closer inspection of these short intervals reveals that the peaks in Γ_r are even shorter than in I_{sat}: Typically, a $\tilde{\Phi}_{fl}$ event is slightly phase shifted with respect to the $\tilde{I}_{sat}$ peak. This is visible in the close-up view of the first peaks of Fig. 8, in Fig. 9, in particular around t = 15.1217s + 80s. The spatial phase shift is transformed into a temporal shift as the structure passes the probe tips due to the poloidal E×B drift. $\tilde{v}_r$ displays a nicely antisymmetric behaviour as a result of the poloidal $\tilde{\Phi}_{fl}$ gradients. However, since the $\tilde{I}_{sat}$ peak is delayed with respect to the $\tilde{\Phi}_{fl}$ peak, the outward component of $\tilde{\Gamma}_r$ is larger than the inward component, and the duration of the $\tilde{\Gamma}_r$ peak is shorter than of the I_{sat} peak.[2]

4.3. COMPARISON OF THE RADIAL TRANSPORT DURING AND IN BETWEEN ELMS

If it is true that, during ELMs, "blobs" (or filaments extended ∥ B) of high density and temperature move radially through the SOL, it is interesting to calculate by what factor the local radial particle and heat fluxes during type I ELMs increase in comparison to their values in between ELMs. This is also of interest to estimate the local fluxes onto wall components which are close (of the order of 10cm) to the LCMS. ELM substructures (and also fluctuation events during L-mode) have indeed been observed to reach the radial position of the main chamber wall in DIII-D [25]. Here, we shall restrict ourselves to the estimate of particle fluxes.

A second question of interest is, whether the turbulent radial E×B transport is sufficient to account for the increased radial transport inferred from transport modelling of ELMs.

In order to answer the above questions, we have subdivided the measurement intervals of the RLP system during three JET discharges into "ELM" time intervals and "inter-ELM" time intervals. We analysed 28 ELM intervals of 0.3-4.5ms length (using either one or both probe tip triples) and 108 inter-ELM intervals of 2-20ms length (using both the innermost and outermost probe tip triples). The end of the ELM intervals was chosen such that either the probe signals had returned to their inter-ELM behaviour or a new ELM started. The length of the inter-ELM intervals is restricted by the requirement that the probes should only move a few millimetres radially within one analysis interval.

For our comparison we use averages over time intervals T of the radial particle flux $\tilde{\Gamma}_r = \tilde{n}\tilde{E}_\theta/B$ (where $\tilde{n}$ is estimated from $\tilde{I}_{sat}$ by neglecting temperature fluctuations and assuming $T_i \equiv T_e \equiv 10eV$ and $\tilde{E}_\theta$ is calculated from two tips measuring $\tilde{\Phi}_{fl}$, as described in section 2.2),

[2] Even if $\tilde{I}_{sat}$ peak and $\tilde{v}_r$ peak were of equal size, the equivalent width of the product peak would be reduced by a factor depending on the precise shape of the peaks.

$$\langle\tilde{\Gamma}_r\rangle_T \equiv \int_{t-T/2}^{t+T/2} \tilde{\Gamma}_r \, dt',$$

and the "effective radial velocity"

$$(v_{r\,\mathrm{eff}})_T \equiv \frac{\langle\tilde{\Gamma}_r\rangle_T}{\int_{t-T/2}^{t+T/2} I_{sat}\, dt'} \tag{1}$$

which has the advantage of being independent of the average temperature [18].

As a measure for the turbulent radial E×B transport in between ELMs we use the averages over the entire analysis intervals (denoted by the subscript 'tot'), $\langle\tilde{\Gamma}_r\rangle_{tot}$ and (υ_{reff})tot. In addition, we calculate running averages over 50μs and 500μs both for ELM and inter-ELM intervals, 50μs being the typical time scale of the individual peaks during an ELM and 500μs being a time scale comparable with the duration of ELMs themselves, as observed on other divertor diagnostics (see, e.g. the ASDEX FDKO signals in section 3). From each analysis interval, we use the maxima of the running averages, $\max(\langle\tilde{\Gamma}_r\rangle_{50/500\mu s})$, $\max((\upsilon_{reff})_{50/500\mu s})$, and the corresponding minima. These values are represented in Fig. 10 together with $\langle\tilde{\Gamma}_r\rangle_{tot}$ and $(\upsilon_{reff})_{tot}$ for the analysis intervals in between ELMs. The radial probe position in this figure is expressed as distance from the separatrix which the corresponding field line has in the torus midplane.

In order to perform a direct comparison between ELM and inter-ELM intervals, we normalise the maxima and minima of the running averages to the averages of the entire interval (for inter-ELM intervals) or to the average of an adjacent inter-ELM interval (for ELM intervals), $\langle\tilde{\Gamma}_r\rangle_{tot}$ and $(\upsilon_{reff})_{tot}$. In this manner we obtain "enhancement factors"

$$F_{50+} \equiv \frac{max(\langle\tilde{\Gamma}_r\rangle_{50\mu s})}{\langle\tilde{\Gamma}_r\rangle_{tot}} \tag{2}$$

$$F_{\Gamma 50} \equiv \frac{min(\langle\tilde{\Gamma}_r\rangle_{50\mu s})}{\langle\tilde{\Gamma}_r\rangle_{tot}} \tag{3}$$

$$F_{\upsilon 50+} \equiv \frac{max(\langle\upsilon_{r\,eff}\rangle_{50\mu s})}{\langle\upsilon_{r\,eff}\rangle_{tot}} \tag{4}$$

$$F_{\upsilon 50} \equiv \frac{min(\langle\upsilon_{r\,eff}\rangle_{50\mu s})}{\langle\upsilon_{r\,eff}\rangle_{tot}} \tag{5}$$

and, likewise, $F_{\Gamma 500+}$, $F_{\Gamma 500-}$, $F_{\upsilon 500+}$ and $F_{\upsilon 500-}$ for the 500μs averages (see Fig. 11). We find that, in between ELMs, the maximum outward particle transport in 500μs intervals is higher by a factor of O(10) than on the average and in 50μs intervals by a factor of O(50). In contrast, during ELMs, we find maximum enhancements of O(300) for the 500μs intervals and of O(2000) for the 50μs

intervals (the factors stated here in the text are geometric averages for the corresponding sets of intervals, to reduce the impact of outliers). Hence the peak radial particle fluxes during ELMs are, on a geometric average, higher by factors of 30-40 than the corresponding peak values in between ELMs.

The enhancement factors of the effective radial velocity during ELMs are lower than for the particle flux. This indicates, that the high radial particle fluxes during ELMs are not only due to higher turbulent radial E×B velocities but also due to peaks in the local density (which were already visible in the I_{sat} raw data, see Fig. 8). This is consistent with the observation in [11] that in larger ELMs (in the sense that $\langle I_{sat} \rangle$ is larger) also higher effective radial velocities are measured.

5. PLASMA POTENTIAL AND BEHAVIOUR OF "BLOBS" IN THE SCRAPE-OFF LAYER

In this section we shall briefly recall the effects generating electric fields $\perp B$ in the SOL, in order to discuss the observed floating potential fluctuation amplitudes and velocities of ELM substructures and "normal" fluctuation events in section 6.1.

In the SOL, the plasma potential in a flux tube can be largely determined by the sheath boundary conditions at the target plates at the ends of that flux tube. The current density onto a target plate can be modeled, in a simple sheath model, as

$$j_{\parallel} = en \left(c_s \quad \frac{\bar{c}_e}{4} \; exp \left(\frac{e\Phi_{pl}}{k_B T_e} \right) \right) \tag{6}$$

(see, e. g., [26]). Here, c_s is the ion sound velocity, $c_s = \sqrt{k_B(T_i + T_e)/(2m_i)}$, and $\bar{c}_e$ is the electron thermal velocity, $c_e = \sqrt{8k_B T_e/(\pi m_e)}$. The target plate potential, as the common reference for all flux tubes, is set = 0. If we calculate the plasma potential from eq. (6), we obtain

$$\Phi_{pl} = -\frac{k_B}{e} T_e \, \mathrm{In} \, \frac{4(c_s - j_{\parallel}/(en))}{\bar{c}_e} . \tag{7}$$

We shall not discuss the range of validity of eq. (6), which is at least limited by the conditions $\Phi_{pl} > 0$ and $j_{\parallel} < enc_s$. For $j_{\parallel} = 0$, the target is at floating potential, i. e.,

$$\Phi_{pl} = -\frac{k_B}{e} \cdot \frac{1}{2} \; (\mathrm{In} \, \frac{T_i + T_e}{T_e} + \mathrm{In} \, \frac{2\pi m_e}{m_i}) \; T_e \equiv \alpha T_e,$$

with $\alpha \approx 2.8 k_B/e$ for deuterium and under the assumption that $T_i = T_e$. This value may be corrected by an additional $(0.5...1)(k_B/e)T_e$, depending on the presheath model. The dependence on the ratio $T_i = T_e$ is comparatively weak, with $T_i = 10\, T_e$ only reducing the numerical factor in α from 2.8 to 2. An electron temperature gradient $\nabla T_e \perp B$ in the SOL therefore generates an electric field ($\alpha \nabla T_e$), which is pointing radially outward for the usual temperature gradient in the plasma edge and hence generates a poloidal E×B drift.

If we now consider fluctuations which are elongated $\parallel B$, the above sheath mechanism still links $\tilde{T}_e$ and $\tilde{\Phi}_{pl}$, which would be in phase, such that (without, for the moment, regarding density

fluctuations) no net energy transport results when averaging over the fluctuation structures. However, in addition, the fluctuations cause current densities $\perp$ B like polarisation currents and fluctuating diamagnetic currents. For illustration, we consider the perturbations of the diamagnetic current $\tilde{j}_\perp$ due to pressure perturbations $\tilde{p}$:

$$\tilde{\boldsymbol{j}}_\perp = - \frac{\nabla \tilde{p} \times \boldsymbol{B}}{B^2}$$

In a non-uniform magnetic field, the divergence of $\tilde{j}_\perp$ does not vanish:

$$\nabla \cdot \tilde{\boldsymbol{j}}_\perp = \nabla \tilde{p} \cdot \left(\nabla \left(\frac{1}{B^2} \right) \times \boldsymbol{B} \right)$$

if the local current density is su ciently low for $\nabla \times$ B to be neglected. Hence, $\nabla \cdot \tilde{j}_\perp$ depends on the component of $\nabla_{\tilde{p}}$ which is perpendicular to the magnetic field and to its gradient. In a tokamak magnetic field, $|B| \approx 1/R$, where R is the major radius. Therefore,

$$\nabla \cdot \tilde{\boldsymbol{j}}_\perp \approx \frac{\partial \tilde{p}}{\partial y} \cdot \frac{2}{BR}, \tag{8}$$

where y = ∇R $\times$ B/B is the direction perpendicular to the major radius and the magnetic field.[3]

In the SOL, $\nabla \cdot \tilde{j}_\perp$ must be balanced by a current density between plasma and target plates. If we assume symmetric current densities onto the target plates $\tilde{j}_\parallel$ at both ends, we obtain

$$-2\, \tilde{j}_\parallel = \int \nabla \cdot \tilde{\boldsymbol{j}}_\perp \, ds, \tag{9}$$

where the integration is $\parallel$ B from one target plate to the other. Using the observation that the SOL fluctuations are highly correlated and of almost constant amplitude along the magnetic eld ([27] and references therein, [28, 29]), and restricting ourselves to a region where $\nabla \cdot \tilde{j}_\perp$ does not vary too much along the magnetic field, like the torus outboard side in a double null divertor configuration, we can set

$$\int \nabla \cdot \tilde{\boldsymbol{j}}_\perp \, ds \approx \frac{\partial \tilde{p}}{\partial y} \cdot \frac{2}{BR} \, L,$$

where L is the length of the flux tube $\parallel$ B. With $\tilde{j}_\parallel$ from eq. (9) in (7), we obtain

$$\Phi_{pl} = \left(\alpha - \frac{k_B}{e} \ln \left(1 + \frac{L}{enc_s RB} \cdot \frac{\partial \tilde{p}}{\partial y} \right) \right) T_e.$$

If, for the moment, we assume T $\equiv$ const, the potential perturbation is out of phase by $\pi/2$ with respect to the pressure perturbation ($\tilde{\Phi}_{pl}$ is largest where $d\tilde{p} / \partial y$ is largest). This mechanism can therefore generate instability in the region of unfavourable magnetic curvature, as was pointed out

[3] Note that eq. (8) is the same expression which results from ∇B and curvature drifts in a single particle picture.

in [30, 31, 32, 33] and, in comparison with experimental data, in [18]. In that investigations, small fluctuations were assumed in order to perform a linear stability analysis.

In contrast, even "normal" SOL fluctuations exhibit considerable relative fluctuation levels, typically > 20-40%. In many observations, the "spikiness" of SOL fluctuations has been noted. They seem to consist of individual "events" [34] or "blobs". This is particularly notable in Langmuir probe measurements of the radial E×B transport, where it has been shown that most of the transport occurs within a comparatively small fraction of time, i.e., due to concentrated "transport events" (see, e.g., [18, 35, 8]), which are also spatially localized [36, 37].

In addition, very at density profiles have been observed several centimetres outside the LCMS in several tokamaks [38, 39], which would imply huge radial transport coeffcients in a diffusive ansatz. Krasheninnikov has pointed out that a blob of plasma with higher pressure than its surroundings and elongated along the magnetic field would indeed start moving radially outward, once it is placed into the SOL in a region of unfavourable magnetic curvature [13], because, as outlined above, the poloidal pressure gradients generate a plasma potential perturbation and hence a radial E×B drift in the centre of the blob.

This model was then extended to include electron temperature [14] and ion temperature perturbations [15], and a detailed comparison between several model predictions and the observed amplitude and radial propagation velocity of ELM substructures for a large sample of ELMs was performed [15]. We shall here only give a brief estimate for the potential perturbation related to the diamagnetic current perturbation in the SOL and the corresponding E×B velocity. We assume a high-pressure blob in a low-pressure background plasma of density n_{bg} and temperature T_{bg}, with n_{blob} and T_{blob} in the centre of the blob, a blob size $\perp$ B of d_{blob}, and evaluate $\tilde{\Phi}_{pl}$ at the edges of the blob, using $n = (n_{bg} + n_{blob}) = 2$, $T = (T_{bg} + T_{blob}) = 2$ and $(\partial\tilde{p} / \partial\theta) = \pm(p_{blob} \quad p_{bg}) = d_{blob}$.

This yields

$$|\tilde{\Phi}\mathrm{pl}| \approx \frac{k_B}{e} \cdot T_e \ln \frac{1 + a}{1 - a}, \tag{10}$$

with $\alpha = (p_{blob} \quad p_{bg})\, L / (enc_s R B d_{blob})$. We shall use the estimate (10) for an approximate comparison of the relations between SOL plasma parameters and potential fluctuation amplitude between this model and the observation in section 6.1.

$$\Phi_{pr} = \Phi_{pl} \qquad \alpha T_e = \quad \frac{k_B}{e} \ln \left(1 \quad \frac{j_{\|}}{enc_s} \right) T_e$$

6. DISCUSSION

6.1. ORIGIN OF THE FINE STRUCTURE AND COMPARISON WITH "NORMAL" SOL FLUCTUATIONS

The use of diagnostics with a resolution of a few millimetres $\perp$ B has revealed that ELMs indeed display substructures on this scale in the SOL of tokamaks. As long as observations with similar spatial resolution

are not available for the edge gradient region inside the LCMS, where ELMs are believed to originate, it is difficult to say whether the observed fine structure is inherent to the instability underlying an ELM, or if it is generated as a secondary effect once plasma from the confinement region is injected into the SOL.

If we compare these substructures to the "events" observed in ohmic or L-mode plasmas or in H-mode between ELMs, the lifetime and poloidal size is rather similar (see section 3.1). The phase shift between $\tilde{\Phi}_{fl}$ and $\tilde{I}_{sat}$ substructures, as described in section 4.2, is also reminiscent of that in "normal" SOL fluctuations [18], and the result that the duration of the $\tilde{\Gamma}_r$ peaks is shorter than that of the I_{sat} peaks was already found in the SOL of ASDEX and Wendelstein 7-AS [40, 41] (in these investigations with poloidal arrays of probe tips it was shown that also the poloidal size of $\tilde{\Gamma}_r$ events is smaller than that of $\tilde{I}_{sat}$ and $\tilde{\Phi}_{fl}$ events).

What differs from "normal" SOL turbulence certainly is the amplitude of the substructures relative to the average values of density and temperature: The relative fluctuation level of I_{sat} in "normal" turbulence does usually not exceed 20-40% in the first few centimetres outside the LCMS. In this respect, the ELM substructures appear to be a prime example for the blobs of high-pressure plasma in a low-pressure background, which were suggested by Krasheninnikov et al. to explain the at gradients in the outer SOL observed in various tokamaks [13, 14].

A further difference between the ELM substructures and "normal" fluctuation events is the uniformity of the poloidal propagation velocity in the latter (see section 3.1). It should be noted here that the poloidal propagation velocity observed by the ASDEX HFD is a velocity of the structures, integrated radially. That method cannot distinguish between a plasma drift velocity and the propagation of a structure (e.g., a wave or a blob) relative to the plasma particles. In contrast, with the JET RLP system, only radial E×B velocities were investigated in section 4. Nevertheless, we can discuss the differences of both velocities between ELM substructures and "normal" fluctuation events: The poloidal velocity of "normal" fluctuations is dominated by the poloidal E×B flow due to the radial electric field, which is generated in the SOL as a result of the radial temperature gradient. 1-3cm outside the separatrix, where the peak intensity contributing to the H_α/D_α signals originates, the radial electron temperature gradient is typically of the order of 10eV/cm, which corresponds, according to section 5, to a poloidal E×B velocity of the order of 1000m/s for B = 2.5T. This is indeed the observed poloidal velocity of "normal" fluctuation structures in ASDEX (see Fig.4). For JET discharges, similar values of the poloidal phase velocity have been reported before [42,43], although in H-mode and closer to the separatrix the conditions may be more complex due to the existence of energetic ions [24].

The poloidal velocity of the ELM substructures in Fig.5 is higher by a factor of 5-10, with the propagation still dominantly in the direction corresponding to a radially outwards directed electric field during the strongest peaks of H_α/D_α emission. A tendency of the poloidal velocity to decrease within the first 100-200s of the ELM is also visible in Fig.5. This behaviour could be explained by a layer of hotter plasma coming into contact with the target plates and thus temporarily increasing the radial electron temperature gradient by a factor of 5-10, however with poloidal inhomogeneities explaining the observed variation in poloidal velocities of the substructures during a single ELM.

Before discussing radial velocities, we should note that a Langmuir probe measuring floating potential is not sensitive to potential perturbations $\tilde{\Phi}_{pl} = \tilde{\alpha} T_e$, as long as the electron temperature uctuations are uniform along the magnetic eld between probe tip and target plate, since the same potential drop $\tilde{\alpha} T_e$ is generated in both sheaths at the probe tip and at the target plate. The probe tip therefore measures only the component of $\tilde{\Phi}_{pl}$ due to fluctuating currents parallel to the magnetic field onto the target plates

$$\Phi_{pr} = \Phi_{pl} \quad \alpha T_e = \frac{k_B}{e} \ln\left(1 \quad \frac{j_{||}}{enc_s}\right) T_e$$

(see section 5). For the case of perturbed diamagnetic currents, this corresponds to expression (10) for the perturbed plasma potential Φ_{pl}.

If we consider the case B = 2.5T, deuterium ions, a background density $n_{bg} = 5 \cdot 10^{18} m^{-3}$, background temperature T_{bg} = 20eV, L = 20m (comparable with the correlation length parallel to the magnetic field of "normal" SOL fluctuations), R = 3m, and a blob size of 2cm, we obtain for $T_i = T_e$ and a typical large "normal" fluctuation event with $n_{blob} = 2n_{bg}$, $T_{blob} = 2T_{bg}$ a potential difference between the blob edges of $\Delta\Phi_{pl} \approx 12V$ and a resulting radial E×B velocity of $v_r \approx 240m/s$. If we keep these values except for $n_{blob} = 5n_{bg}$, $T_{blob} = 5T_{bg}$ for the case of an ELM substructure, we obtain $\Delta\Phi_{pl} \approx 75V$ and $\upsilon_r \approx 1500m/s$. The case of $n_{blob} = 5n_{bg}$, $T_{e,\,blob} = 2T_{bg}$, $T_{i,\,blob} = 10T_{bg}$ yields only $\Delta\Phi_{pl} \approx 40V$ and $\upsilon_r \approx 860m/s$, since the factor T_e has a larger influence on the result than T_i in the argument of the logarithm in eq. (10). Radial velocities of 1000-2000m/s for ELM substructures have consistently been observed by calculating the radial E×B velocity [9, 12] and the time delay between the peaks on radially displaced probe tips [12, 15].

From the similarity in the relative phase between and Isat fluctuations between "normal" SOL fluctuations and ELM substructures (see section 4.2) and from the fact that the amplitude of measured floating potential fluctuations can in both cases be described in the framework of the same model, we conclude that the same mechanism is underlying the behaviour of the ELM substructures in the SOL and the "normal" SOL fluctuations.

Concerning the phase between density and electron temperature fluctuations during the ELM substructures, different results were found in the measurements at JET (n and $\tilde{T}_e$ in phase [11]) and at DIII-D (hardly any correlation between n and $\tilde{T}_e$ from conditional averaging during ELMs, in contrast to events during "normal" fluctuations [10]), however with different techniques for the measurement of $\tilde{T}_e$.

Since plasma of unusually high density and temperature is present in the SOL during ELMs, they might also serve as a "laboratory" to investigate the turbulence dynamics typical for the SOL over a wider range of parameters than under normal SOL conditions. This could include a more detailed investigation of the changes in relative phase between $\tilde{n}$, $\tilde{T}_e$ and $\tilde{\Phi}_{pl}$.

6.2. RADIAL TRANSPORT DURING AND IN BETWEEN ELMS

As we have discussed in section 6.1, our computation of the turbulent radial particle flux can be taken as a realistic estimate in spite of the neglect of temperature fluctuations. We then find local

transport enhancement factors of O(300) (geometric average) for 500μs ELM intervals relative to the average inter-ELM transport, however with a large scatter between di erent ELMs (see section 4.3) and slightly decreasing close to the separatrix (which could be a selection effect, since a larger fraction of ELMs had to be excluded from the analysis due to probe tip emission when the probe head was close to the LCMS). For transport modelling of type I ELMs in ASDEX Upgrade with the B2-EIRENE package, Coster et al. had to increase the transport coeffcients around the separatrix by a factor of 50 for 1ms to describe the transport effect of an ELM [44]. Similarly, Kallenbach et al. find in EDGE2D/NIMBUS modelling of type I ELMs in JET that they have to increase the particle diffusion coeffcients by a factor of 20 for 1ms [45]. No transport modeling for ELMs exists for the far SOL several centimetres outside the separatrix to compare with. We can conclude, however, that the increase in turbulent radial E×B transport during ELMs in comparison with the inter-ELM level is at least sufficient to explain the transport increase which is modeled in transport codes by increased transport coeffcients to describe the effect of ELMs. This is also consistent with the conclusion of Counsell et al. from the evolution of edge Thomson density and electron temperature profiles that the energy loss from the pedestal region of MAST during ELMs is purely convective [6].

6.3. FOOTPRINTS OF SUBSTRUCTURES ON THE DIVERTOR PLATES

Recently, fast infrared camera observations of the divertor plates in ASDEX Upgrade showed the existence of a spatial substructure of the power flux onto the plates significantly outside the strike line marking the intersection of the separatrix with the target plate during type I ELMs [16]. While two or three radial peaks had been observed in target plate power flux measurements during ELMs in JT-60U before [46], it was now demonstrated in [16], that the radial positions and number of these substructures vary between individual ELMs, they are not toroidally symmetric but display a pattern which would result from a blob with approximately circular shape in the midplane due to the magnetic shear. For the case of “normal” fluctuations, it has been demonstrated that magnetic shear can indeed distort the poloidal-radial cross section (and thus also the toroidal-radial cross section) of the fluctuation structures due to their large correlation length parallel to the magnetic field [29, 47]. We would therefore interpret the thermographically observed ELM substructures on target plates with lifetimes below 100μs as the footprints of structures like those observed in the SOL of the main plasma with the ASDEX HFD and the JET RLP systems.

Models assessing the impact of ELMs on the lifetime of divertor target materials, like that presented in [48], should therefore consider that the ELM thermal load to the divertor plates can locally also have a temporal substructure within the total ELM duration of the order of 500μs. This can be seen on divertor Langmuir probe signals with sufficiently high sampling rate (see, e.g., [49, Fig.7]). Qualitatively, the erosion threshold for tungsten and carbon plates was shown to be lowered if the duration of model ELMs consisting of a single peak with given shape and energy deposition was reduced [48, Figs.9 and 10].

CONCLUSIONS

We have directly observed the poloidal ne structure of ELMs in the edge and SOL of ASDEX with a resolution of 6mm and a baselength fo 4.5 cm. An ELM usually consists of substructures or "blobs" with a poloidal size of few centimetres, similar to the "events" observed in the "normal" fluctuations in between ELMs. However, the poloidal velocity of the ELM substructures is higher by a factor of 10-20 and less uniform than during "normal" SOL turbulence.

The comparison of poloidal and radial propagation velocities of ELM substructures and "normal" SOL fluctuations with the values of stationary and fluctuating plasma potentials estimated from a simple sheath model and the common behaviour of relative phase between I_{sat} and Φ_{fl} led us to conclude that these phenomena can be described in a unified picture based on the target plate instability/blob propagation model.

For ELMs on MAST it was shown on fast camera snapshots that the ELM substructures are arranged rather parallel to the magnetic field [17]. Conducting the comparison with "normal" fluctuations further could include an investigation, to which precision this is the case and whether the correlation is as high as it was found for the "normal" SOL turbulence (for ASDEX, see [18], for JET, see [28]).

We have estimated the local turbulent radial E B transport during type I ELMs from ion saturation and floating potential measurements in the JET SOL. This transport is concentrated on scales of a few centimetres (derived from the differences in the signals of two sets of probe tips), i.e. on similar scales as the peaks in I_{sat} signals, and locally in time intervals of 10-50μs.

The radial distance traveled by the plasma while such a blob is detected by the probe tips can reach 10cm, and the lifetime of the blob may be longer due to its propagation past the probe tips, as it is observed in the ASDEX H_α/D_α fluctuation data. These directly measured radial E×B velocities (see also [12]) are therefore consistent with the observation of increased density 10cm outside the separatrix, e.g. in MAST [6] or ASDEX Upgrade [50], with the phenomenon that only half of the ELM energy loss is found on the targets in many discharges in JET and ASDEX Upgrade [49, Fig. 4] or, for an overview, [51], and with the values of υ_r expected in the context of the target plate instability/ blob model (see section 6.1 and [10, 15]) and also found from the average delay of the I_{sat} peak at different radial positions of JET limiter probes [15]. In addition, the order of magnitude of turbulent radial E×B transport increase during ELMs as compared with inter-ELM intervals is consistent with the transport increase used in transport models to describe the effect of ELMs.

There exist different results about the relative phase between density and electron temperature fluctuations during ELM substructures [10, 11]. A more detailed investigation of this topic, including a comparison with the behaviour of "normal" fluctuations, would be interesting, in order to compare the results with SOL turbulence models in a parameter regime not normally found in the SOL. However, a more detailed investigation of Langmuir probes under non-stationary conditions may also be required to interpret such measurements correctly [15].

Taking into account the indications that the ion temperature may significantly exceed the electron temperature [24], a time-resolved measurement of the ion temperature during ELMs would be important in order not to possibly miss the major fraction of radial heat transport.

In order to decide experimentally whether the observed fine structure is based on the instability underlying the ELM and hence already exists during the birth of ELMs, or whether this fine structure is only generated in the SOL by those mechanisms also responsible for the "normal" SOL turbulence, diagnostics with comparable spatial and temporal resolution would be required for the steep gradient region inside the LCMS, where ELMs originate.

ACKNOWLEDGEMENTS

We thank S. Davies, K. Erents, H. Guo and R. Monk for stimulating discussions and for their help in running the JET RLP systems and determining probe positions and radial profiles, W. Fundamenski, C. Silva and T. Eich for their important comments, H. Niedermeyer and A. Rudyj for clarifying discussions on the interpretation of the ASDEX H_α data and H. Scholz and G. Neill for their invaluable contributions to building and maintaining the diagnostic systems used in these experiments.

REFERENCES

[1]. WAGNER, F. et al., Phys. Rev. Lett. **49** (1982) 1408, http://prola.aps.org/pdf/PRL/v49/i19/- p1408 1.

[2]. ASDEX TEAM, Nucl. Fusion **29** (1989) 1959.

[3]. ZOHM, H., Plasma Phys. Controlled Fusion **38** (1996) 105, http://www.iop.org/EJ/article/-0741-3335/38/2/001/p602r1.pdf.

[4]. HILL, D. N., J. Nucl. Mater. **241-243** (1997) 182, Proceedings of the 12th International Conference on Plasma-Surface Interactions in Controlled Fusion Devices, Saint-Raphanel, France, 20-24 May 1996.

[5]. ELMs special issue, Plasma Phys. Controlled Fusion **45**(9) (September 2003), http://-www.iop.org/EJ/toc/0741-3335/45/9.

[6]. COUNSELL, G. F., AHN, J.-W., AKERS, R., ARENDS, E., BUTTERY, R., FIELD, A. R., GRYAZNEVICH, M., HELANDER, P., KIRK, A., MEYER, H., VALOVIC, M., WILSON, H. R., YANG, Y., and MAST TEAM, Plasma Phys. Controlled Fusion **44** (2002) B23, Invited papers from the 29th European Physical Society Conference on Plasma Physics and Controlled Fusion, Montreux, Switzerland, 17-21 June 2002, http://stacks.iop.org/PPCF/44/B23.

[7]. AHN, J.-W., COUNSELL, G. F., KIRK, A., TABASSO, A., HELANDER, P., and YANG, Y., Progress in SOL and divertor studies on the MAST tokamak, in 29th EPS Conference on Plasma Physics and Controlled Fusion (Montreux), edited by BEHN, R. and VARANDAS, C., volume 26B, European Physical Society, 2002, paper P-1.055, http://epsppd.epfl.ch/Montreux/pdf/-P1_055.pdf.

[8]. HIDALGO, C., PEDROSA, M. A., GONC ALVES, B., SILVA, C., BALB IN, R., HRON, M., ERENTS, K., MATTHEWS, G., and LOARTE, A., Edge localized modes and fluctuations in the JET SOL region, in 29th EPS Conference on Plasma Physics and Controlled Fusion (Montreux), edited by BEHN, R. and VARANDAS, C., volume 26B, European Physical Society, 2002, paper O-2.05, http://epsppd.epfl.ch/Montreux/pdf/O2_05.pdf.

[9]. ENDLER, M., DAVIES, S., GARC IA-CORT ES, I., MATTHEWS, G. F., ASDEX TEAM, and JET TEAM, The ne structure of ELMs, in 29th EPS Conference on Plasma Physics and Controlled Fusion (Montreux), edited by BEHN, R. and VARANDAS, C., volume 26B, European Physical Society, 2002, paper O-3.24, http://epsppd.ep .ch/Montreux/pdf/O3 24.pdf.

[10] RUDAKOV, D. L., BOEDO, J. A., MOYER, R. A., KRASHENINNIKOV, S., LEONARD, A. W., MAHDAVI, M. A., McKEE, G. R., PORTER, G. D., STANGEBY, P. C., WATKINS, J. G., WEST, W. P., WHYTE, D. G., and ANTAR, G., Plasma Phys. Controlled Fusion **44** (2002) 717, http://stacks.iop.org/PPCF/44/717.

[11]. SILVA, C., GONC ALVES, B., HIDALGO, C., ERENTS, K., LOARTE, A., MATTHEWS, G., and PEDROSA, M., Determination of the particle and energy fluxes in the JET far SOL during ELMs using the reciprocating probe diagnostic, Proceedings of the 16th International Conference on Plasma Surface Interactions in Controlled Fusion Devices, Portland, Maine, USA, 24{28 May 2004, paper O-25, http://www.psfc.mit.edu/psi16/talks/O-25%20Silva.pdf, submitted to J. Nucl. Mater.

[12]. GONC ALVES, B., HIDALGO, C., PEDROSA, M. A., SILVA, C., BALB IN, R., ERENTS, K., HRON, M., LOARTE, A., and MATTHEWS, G., Plasma Phys. Controlled Fusion **45** (2003) 1627, http://www.iop.org/EJ/article/0741-3335/45/9/305/p30905.pdf.

[13]. KRASHENINNIKOV, S. I., Phys. Lett. A **283** (2001) 368.

[14]. D'IPPOLITO, D. A., MYRA, J. R., and KRASHENINNIKOV, S. I., Phys. Plasmas **9** (2002) 222.

[15]. FUNDAMENSKI, W., SAILER, W., and JET EFDA CONTRIBUTORS, Plasma Phys. Controlled Fusion **46** (2004) 233, http://stack.iop.org/PPCF/46/233.

[16]. EICH, T., HERRMANN, A., NEUHAUSER, J., and ASDEX UPGRADE TEAM, Phys. Rev. Lett. **91** (2003) 195003.

[17]. KIRK, A., WILSON, H. R., COUNSELL, G. F., AKERS, R., COWLEY, S. C., DOWLING, J., LLOYD, B., PRICE, M., WALSH, M., and MAST TEAM, Phys. Rev. Lett. **92** (2004) 245002.

[18]. ENDLER, M., GIANNONE, L., HOLZHAUER, E., NIEDERMEYER, H., RUDYJ, A., THEIMER, G., TSOIS, N., and ASDEX TEAM, Nucl. Fusion **35** (1995) 1307, http://-www.iop.org/EJ/article/0029-5515/35/11/I01/nfv35i11p1307.pdf.

[19]. ENDLER, M., Experimentelle Untersuchung und Modellierung elektrostatischer Fluktuationen in den Abschnalschichten des Tokamak ASDEX und des Stellarators Wendelstein 7-AS, PhD thesis, Technische Universitnat Mnunchen, 1994, Max-Planck-Institut fnur Plasmaphysik report IPP III/197.

[20]. DAVIES, S. J., ERENTS, S. K., LOARTE, A., GUO, H. Y., MATTHEWS, G. F., McCORMICK, K., and MONK, R. D., Contrib. Plasma Phys. **36** (1996) 117, Proceedings of the Second International Workshop on Electrical Probes in Magnetized Plasmas, 4-6 October 1995, The Harnack-House, Berlin, Germany.

[21]. GARC IA-CORT ES, I., ENDLER, M., LOARTE, A., DAVIES, S. J., ERENTS, S. K., GUO, H., HIDALGO, C., LINGERTAT, J., MART IN-SOL IS, J. R., MATTHEWS, G. F., VAN MILLIGEN, B., MONK, R. D., SIMONINI, R., and TARONI, A., Turbulence studies in the JET scrape-o layer plasmas, in 24th EPS Conference on Controlled Fusion and Plasma Physics (Berchtesgaden), edited by SCHITTENHELM, M., BARTIROMO, R., and WAGNER, F., volume 21A, part I, pp. 109-112, European Physical Society, 1997.

[22]. DAVIES, S. J., ENDLER, M., ERENTS, S. K., GARC IA-CORT ES, I., GUO, H. Y., HIDALGO, C., LOARTE, A., MARTIN-SOLIS, R., MATTHEWS, G. F., McCORMICK, K., MONK, R. D., and STANGEBY, P. C., Contrib. Plasma Phys. **38** (1998) 61, Proceedings of the Third International Workshop on Electrical Probes in Magnetized Plasmas, 22-25 September 1997, Magnus-House, Berlin, Germany.

[23]. PFEIFFER, U., ENDLER, M., BLEUEL, J., NIEDERMEYER, H., THEIMER, G., and W7-AS TEAM, Contrib. Plasma Phys. **38** (1998) 134, Proceedings of the Third International Workshop on Electrical Probes in Magnetized Plasmas, 22-25 September 1997, Magnus-House, Berlin, Germany.

[24]. FUNDAMENSKI, W., SIPILnA, S., MATTHEWS, G. F., RICCARDO, V., ANDREW, P., EICH, T., INGESSON, L. C., KIVINIEMI, T., KURKI-SUONIO, T., PHILIPPS, V., and CONTRIBUTORS TO THE EFDA JET WORK PROGRAMME, Plasma Phys. Controlled Fusion **44** (2002) 761, http://stacks.iop.org/PPCF/44/761, Special issue on the IAEA Technical Committee Meeting on Divertor Concepts.

[25]. RUDAKOV, D. L., BOEDO, J. A., MOYER, R. A., DOERNER, R. P., HOLLMANN, E. M., KRASHENINNIKOV, S., BROOKS, N. H., EVANS, T. E., MAHDAVI, M. A., WEST, W. P., WONG, C. P. C., FENSTERMACHER, M. E., GROTH, M., LASNIER, C. J., McKEE, G. R., WHYTE, D. G., McLEAN, A., STANGEBY, P. C., WAMPLER, W. R., and WATKINS, J. G., Far scrape-o layer and near wall plasma studies in DIII-D, presented at the 16th International Conference on Plasma Surface Interactions in Controlled Fusion Devices, Portland, Maine, USA, 24-28 May 2004, paper O-24, http://www.psfc.mit.edu/psi16/talks/O-24%20Rudakov.pdf.

[26]. STANGEBY, P. C., The plasma sheath, in Physics of Plasma-Wall Interactions in Controlled Fusion, edited by POST, D. E. and BEHRISCH, R., volume 131 of NATO ASI series, Series B, Physics, pp. 41-97, New York, 1986, Plenum Press.

[27]. ENDLER, M., J. Nucl. Mater. **266-269** (1999) 84, Proceedings of the Thirteenth International Conference on Plasma-Surface Interactions in Controlled Fusion Devices, San Diego, CA, USA, 18-22 May 1998.

[28]. THOMSEN, H., BLEUEL, J., ENDLER, M., CHANKIN, A., ERENTS, S. K., MATTHEWS, G. F., and JET TEAM, Phys. Plasmas **9** (2002) 1233.

[29]. BLEUEL, J., ENDLER, M., NIEDERMEYER, H., SCHUBERT, M., THOMSEN, H., and W7-AS TEAM, New J. Phys. **4** (2002) 38, http://stacks.iop.org/1367-2630/4/38.

[30]. CHEN, F. F., Plasma Phys. **7** (1965) 399.

[31]. KUNKEL, W. B. and GUILLORY, J. U., Interchange stabilization by incomplete line-tying, in Proc. 7th Int. Conf. on Phenomena in Ionized Gases, volume 2, pp. 702-706, Belgrade, 1965.

[32]. NEDOSPASOV, A. V., Soviet Journal of Plasma Physics **15** (1989) 659.

[33]. GARBET, X., LAURENT, L., ROUBIN, J.-P., and SAMAIN, A., Nucl. Fusion **31** (1991) 967.

[34]. THEIMER, G., ENDLER, M., GIANNONE, L., NIEDERMEYER, H., and ASDEX TEAM, Individual event analysis: A new tool for the investigation of structures in turbulence, in Transport, Chaos and Plasma Physics 2, edited by BENKADDA, S., DOVEIL, F., and ELSKENS, Y., volume 9 of Advanced Series in Nonlinear Dynamics, pp. 89-92, Singapore, New Jersey, London, Hong Kong, 1996, World Scientific, Proceedings of the Second International Workshop on Transport, Chaos and Plasma Physics, 10-22 July 1996, Marseille, France.

[35]. ANTAR, G. Y., KRASHENINNIKOV, S. I., DEVYNCK, P., DOERNER, R. P., HOLLMANN, E. M., BOEDO, J. A., LUCKHARDT, S. C., and CONN, R. W., Phys. Rev. Lett. **87** (2001) 065001.

[36]. THEIMER, G., Charakterisierung transportrelevanter turbulenter elektrostatischer Fluktuationen in der Abschnalschicht des Tokamaks ASDEX mittels Darstellung als Superposition von raum- zeitlich lokalisierten Ereignissen, PhD thesis, Technische Universitnat Mnunchen, 1997, IPP report III/223, Max-Planck-Institut fnur Plasmaphysik, Garching.

[37]. ENDLER, M., GIANNONE, L., McCORMICK, K., NIEDERMEYER, H., RUDYJ, A., THEIMER, G., TSOIS, N., ZOLETNIK, S., ASDEX TEAM, and JET TEAM, Turbulent fluctuations in the scrape-o layer of the ASDEX tokamak and the W7-AS stellarator, in 21st EPS Conference on Controlled Fusion and Plasma Physics (Montpellier), edited by JOFFRIN, E., PLATZ, P., and STOTT, P. E., volume 18B, part II, pp. 874-877, European Physical Society, 1994.

[38]. BOSCH, H.-S., NEUHAUSER, J., SCHNEIDER, R., FIELD, A., HERRMANN, A., LIEDER, G., JUNKER, W., PITCHER, C. S., REITER, D., BRAAMS, B., and ASDEX UPGRADE TEAM, J. Nucl. Mater. **220-222** (1995) 558.

[39]. UMANSKY, M. V., KRASHENINNIKOV, S. I., LaBOMBARD, B., and TERRY, J. L., Phys. Plasmas **5** (1998) 3373.

[40]. ENDLER, M., GIANNONE, L., McCORMICK, K., NIEDERMEYER, H., RUDYJ, A., THEIMER, G., TSOIS, N., ZOLETNIK, S., ASDEX TEAM, and W7-AS TEAM, Physica Scripta **51** (1995) 610.

[41]. BLEUEL, J., Elektrostatische Turbulenz am Plasmarand des Stellarators Wendelstein 7-AS, PhD thesis, Technische Universitnat Mnunchen, 1998, Max-Planck-Institut fnur Plasmaphysik report IPP III/235.

[42]. GARC IA-CORT ES, I., BALB IN, R., LOARTE, A., BLEUEL, J., CHANKIN, A., DAVIES, S. J., ENDLER, M., ERENTS, S. K., HIDALGO, C., MATTHEWS, G. F., van MILLIGEN, B., and THOMSEN, H., Plasma Phys. Controlled Fusion **42** (2000) 389.

[43]. GARC IA-CORT ES, I., LOARTE, A., BALB IN, R., BLEUEL, J., CHANKIN, A., DAVIES, S. J., ENDLER, M., ERENTS, S. K., HIDALGO, C., MATTHEWS, G. F., and THOMSEN, H., J. Nucl. Mater. **290-293** (2001) 604, Proceedings of the 14th PSI, 2000.

[44]. COSTER, D. P., SCHNEIDER, R., NEUHAUSER, J., BRAAMS, B., and REITER, D., Contrib. Plasma Phys. **36** (1996) 150.

[45]. KALLENBACH, A., ANDREW, Y., BEURSKENS, M., CORRIGAN, G., EICH, T., JACHMICH, S., KEMPENAARS, M., KOROTKOV, A., LOARTE, A., MATTHEWS, G., MONIERGARBET, P., SAIBENE, G., SPENCE, J., SUTTROP, W., and JET EFDA CONTRIBUTORS, Plasma Phys. Controlled Fusion **46** (2004) 431, http://stacks.iop.org/PPCF/46/431.

[46]. ASAKURA, N., SAKURAI, S., NAITO, O., ITAMI, K., MIURA, Y., HIGASHIJIMA, S., KOIDE, Y., and SAKAMOTO, Y., Plasma Phys. Controlled Fusion **44** (2002) A313.

[47]. BRUCHHAUSEN, M., BURHENN, R., ENDLER, M., KOCSIS, G., POSPIESZCZYK, A., ZOLETNIK, S., and W7-AS TEAM, Plasma Phys. Controlled Fusion **46** (2004) 489, http://stacks.iop.org/PPCF/46/489.

[48]. FEDERICI, G., LOARTE, A., and STROHMAYER, G., Plasma Phys. Controlled Fusion **45** (2003) 1523.

[49]. HERRMANN, A., EICH, T., JACHMICH, S., LAUX, M., ANDREW, P., BERGMANN, A., LOARTE, A., MATTHEWS, G., NEUHAUSER, J., ASDEX UPGRADE TEAM, and CONTRIBUTORS TO EFDA-JET WORK PROGRAMME, J. Nucl. Mater. **313-316** (2003) 759, Proceedings of Plasma-Surface Interactions in Controlled Fusion Devices 15, Gifu, Japan, 26-31 May 2002.

[50]. NUNES, I., CONWAY, G. D., MANSO, M., MARASCHEK, M., SERRA, F., SUTTROP, W., CFN TEAM, and ASDEX UPGRADE TEAM, Study of ELMs on ASDEX Upgrade using re ectometry measurements with high temporal and spatial resolution, in 29th EPS Conference on Plasma Physics and Controlled Fusion (Montreux), edited by BEHN, R. and VARANDAS, C., volume 26B, European Physical Society, 2002, paper O-5.06, http://epsppd.ep .ch/Montreux/-pdf/O5_06.pdf.

[51]. EICH, T., HERRMANN, A., PAUTASSO, G., ANDREW, P., ASKURA, N., BOEDO, J. A., FENSTERMACHER, M. E., FUCHS, J. C., FUNDAMENSKI, W., FEDERICI, G., GAUTHIER, E., GONC ALVES, B., GRUBER, O., KIRK, A., LEONARD, A. W., LOARTE, A., MATTHEWS, G., NEUHAUSER, J., PITTS, R. A., RICCARDO, V., and SILVA, C., Power deposition onto plasma facing components in poloidal divertor tokamaks during type-I ELMs and disruptions, Proceedings of the 16th International Conference on Plasma Surface Interactions in Controlled Fusion Devices, Portland, Maine, USA, 24-28 May 2004, paper R-3, http://www.psfc.mit.edu/psi16/talks/R-3%20Eich.pdf, submitted to J. Nucl. Mater.

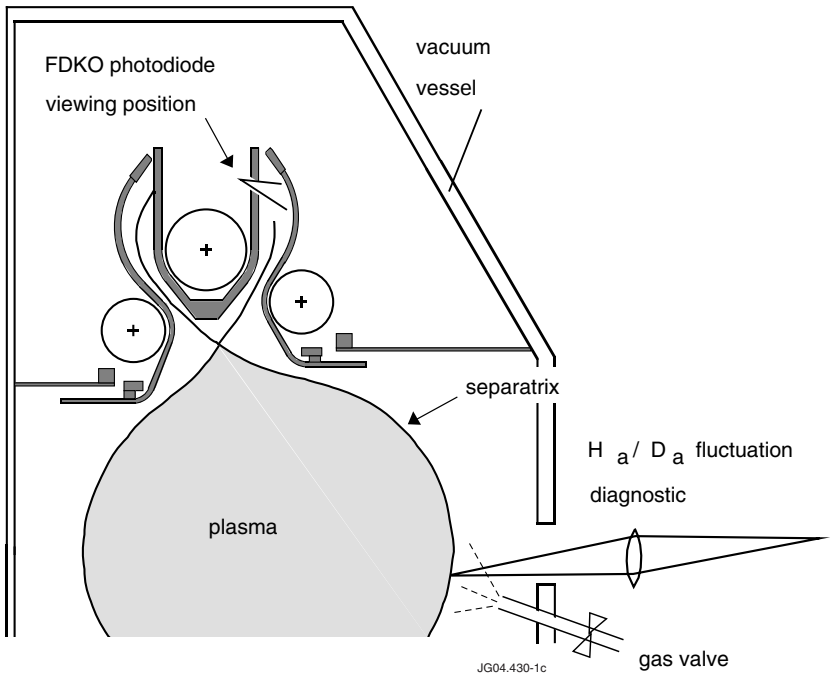

Figure 1: Arrangement of the H_α /D_α fluctuation diagnostic in the midplane and of the FDKO photodiode in the divertor of the ASDEX tokamak. The two diagnostics shown here in the same poloidal cross section were not located at the same toroidal position.

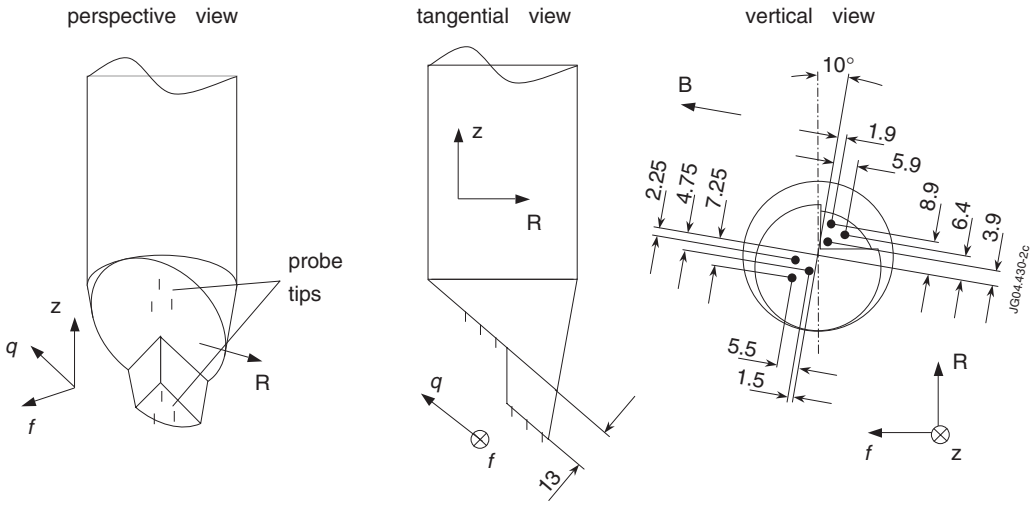

Figure 2: Probe head used for fluctuation measurements on a reciprocating drive in the JET tokamak. Two groups of three probe tips were arranged at two radial positions. The tips of each triple were approximatly at the same radial position and at different poloidal positions. They were arranged in triangles to avoid shadowing. The tips were cylindrical and manufactured from graphite with 1.5mm diameter. All lengths in this figure are given in millimetres.

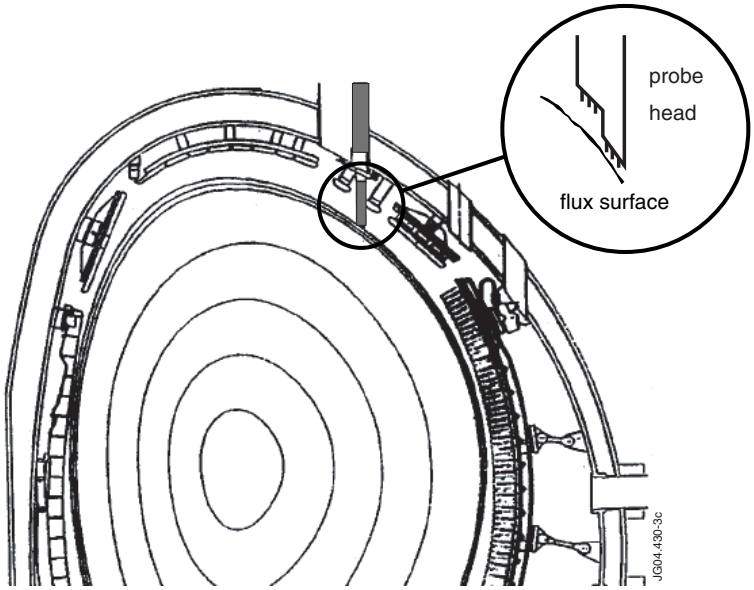

Figure 3: Arrangement of the reciprocating Langmuir probe (RLP) system on JET.

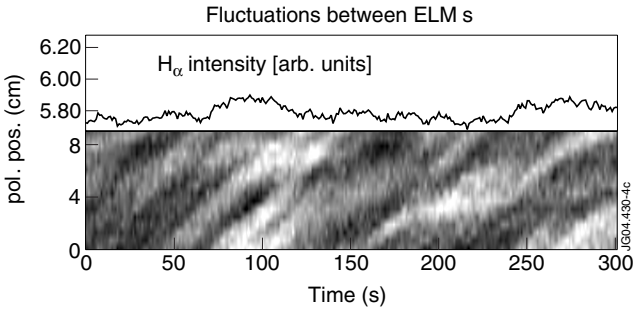

Figure 4: Grey scale image of the 16 poloidally displaced channels of the HFD at ASDEX for a time interval in between ELMs, showing the "normal" fluctuations and their typical poloidal size, lifetime and poloidal propagation (bottom). The time trace from one of the 16 channels is depicted in the top panel.

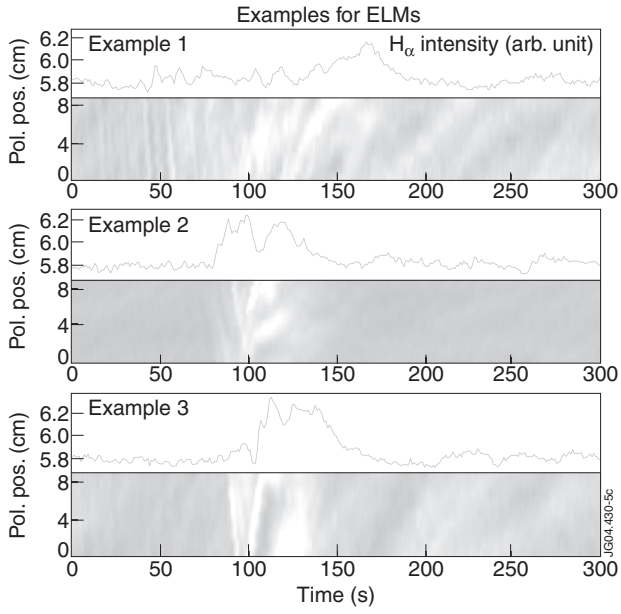

Figure 5: Same as in Fig. 4, but during three ELMs. The ELMs exhibit substructures on a time scale of 20s, and their poloidal velocity is much higher than for "normal" fluctuations. In addition, not all of the substructures move in the same direction.

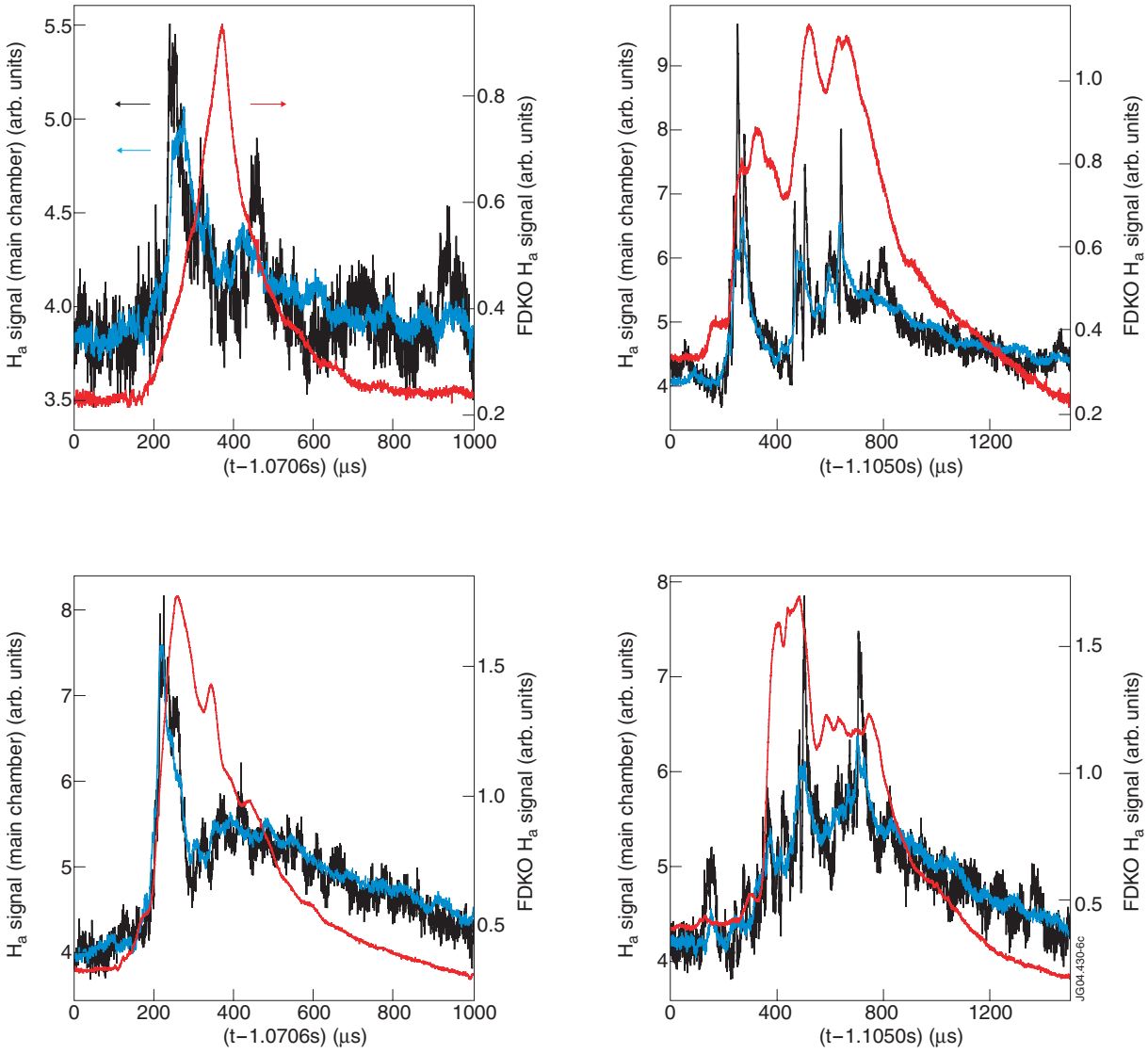

Figure 6. Comparison between signals of the H_a/D_a fluctuation diagnostic in the midplane of ASDEX (black: single channel; blue: average over 8 channels, corresponding to a poloidal region of 9cm) and the "FDKO" H_a/D_a monitor in the upper divertor (red) for four different ELMs in one discharge.

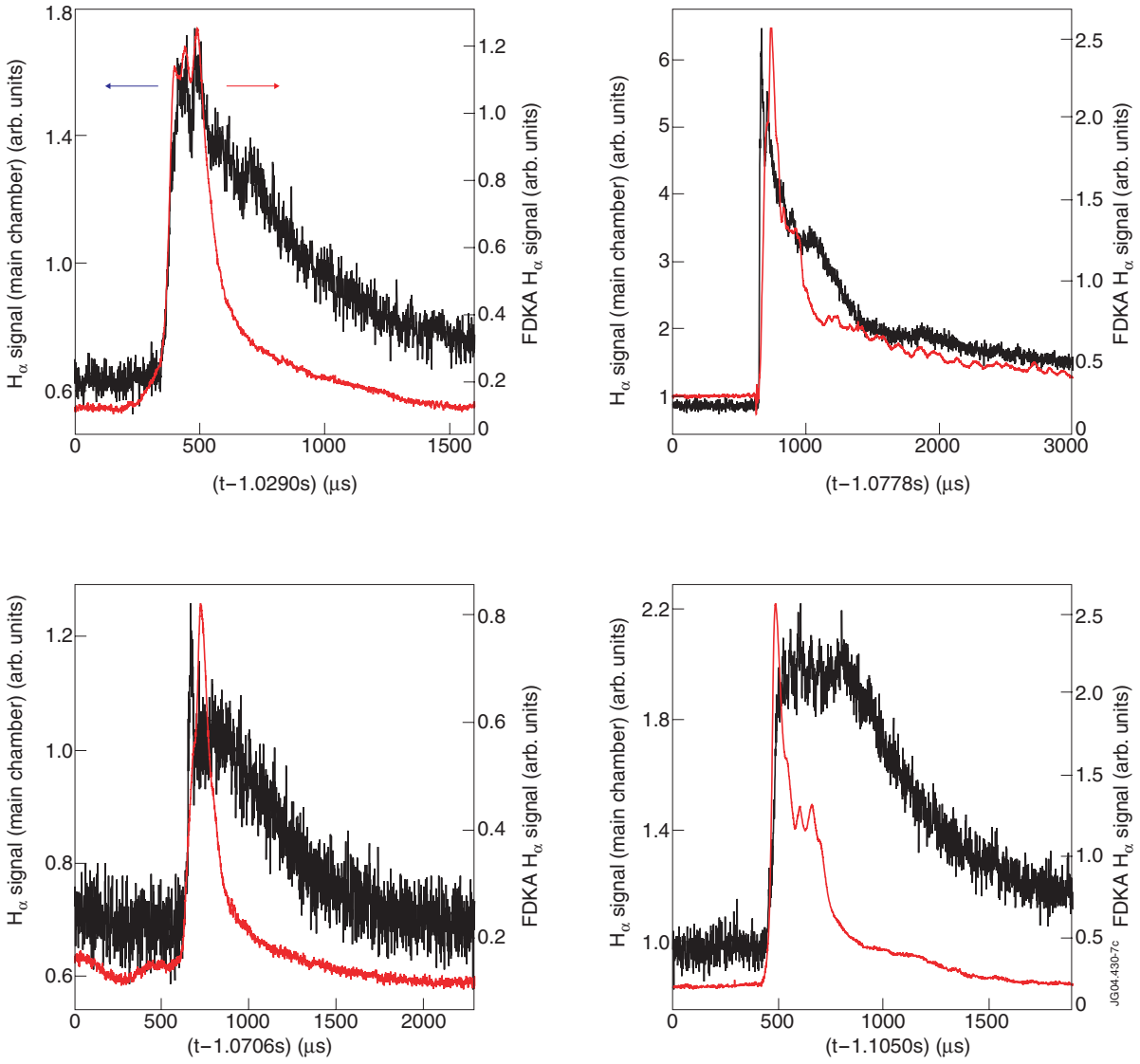

Figure 7. Comparison between signals of the H_α/D_α fluctuation diagnostic in the midplane of ASDEX without puffing in gas into the observed region (black) and the "FDKO" H_α/D_α monitor in the upper divertor (red) for four different ELMs in one discharge. Without the constant gas puffing, the midplane signal is dominated by the change in recycling during the ELM. Fast substructures like those visible in Fig. 6 are in this case hardly discernible.

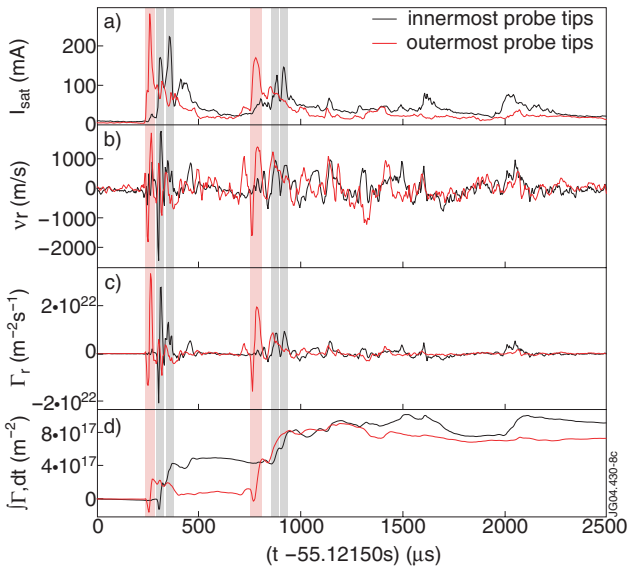

Figure 8. Measurements of the two Langmuir probe tip triples on the RLP system during one ELM in a JET 12MW NBI discharge. (a) I_{sat}; (b) radial E×B velocity (calculated from the poloidal difference in floating potential, neglecting temperature flucutations); (c) resulting fluctuating radial particle transport Γ_r (assuming $T_i \equiv T_e$ 10eV for the calculation of n from I_{sat}); (d) time integral of Γ_r. The vertical grey and rose bars are intended to help relating the behaviour of the different quantities for the strongest radial transport events. The innermost probe tips are approximately 3.5 midplane-cm outside the LCMS, the outermost probe tips 0.7 midplane-cm farther out.

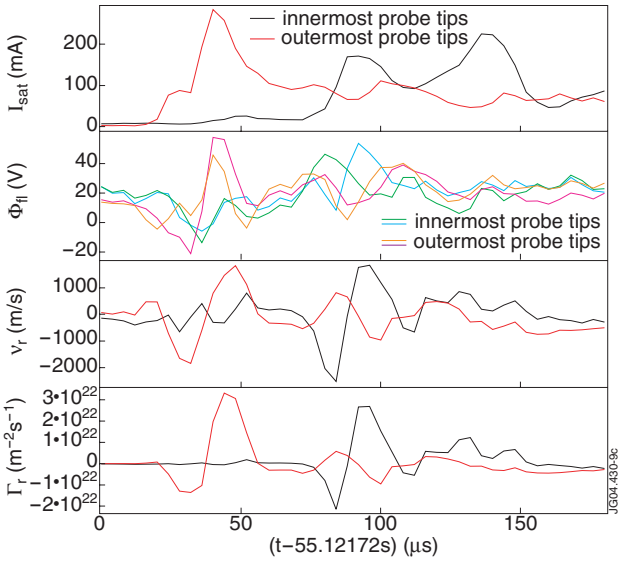

Figure 9: Enlarged view of the first peaks in Fig. 8. In contrast to Fig. 8, the $\tilde{\Phi}_{fl}$ signals are displayed in the second panel, and $\int\tilde{\Gamma}_r dt$ is omitted. The sequence of probe tips in poloidal E×B drift direction is (orange, red, magenta; green, black, cyan).

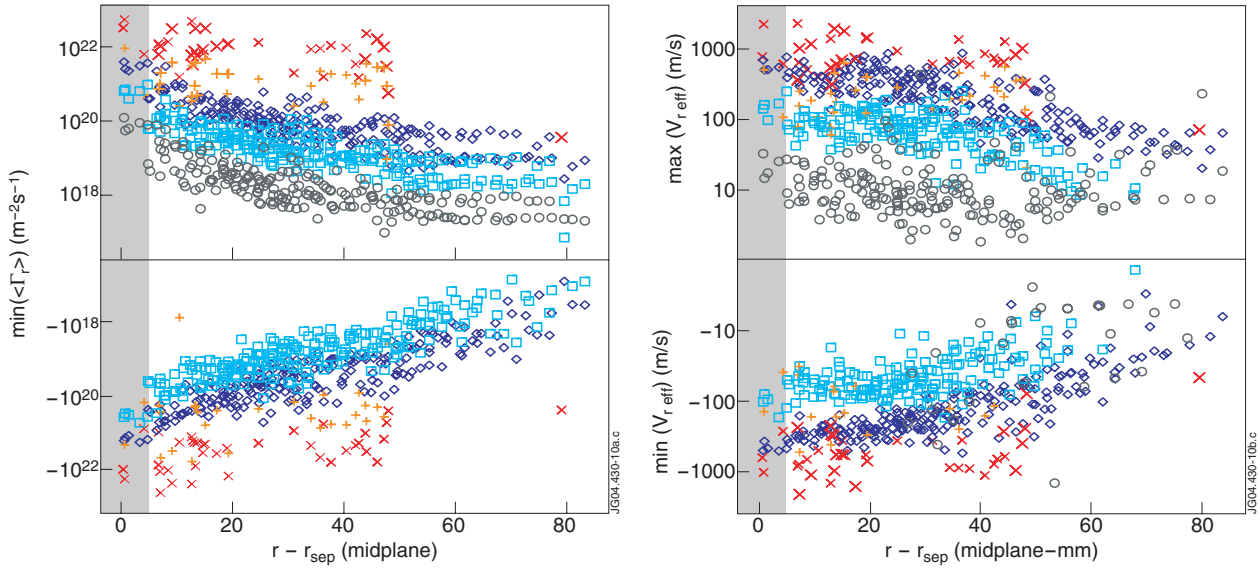

Figure 10: Maximum and minimum values for running averages of the radial particle transport $\langle\Gamma_r\rangle_T$ (left) and the effective radial velocity (v_{reff})T as defined in eq. 1 (right) during ELMs and between ELMs as a function of the probe position in the JET SOL (the separatrix location and its uncertainty is indicated by the grey bar). The symbols/colours are for ×/red: ELM intervals, 50μs averages; +/orange: ELM intervals, 500μs averages; ◇/blue: inter-ELM intervals, 50μs averages; □/cyan: inter- ELM intervals, 500μs averages; ○/grey: inter-ELM intervals, entire analysis interval (i. e., 2-20ms averages).

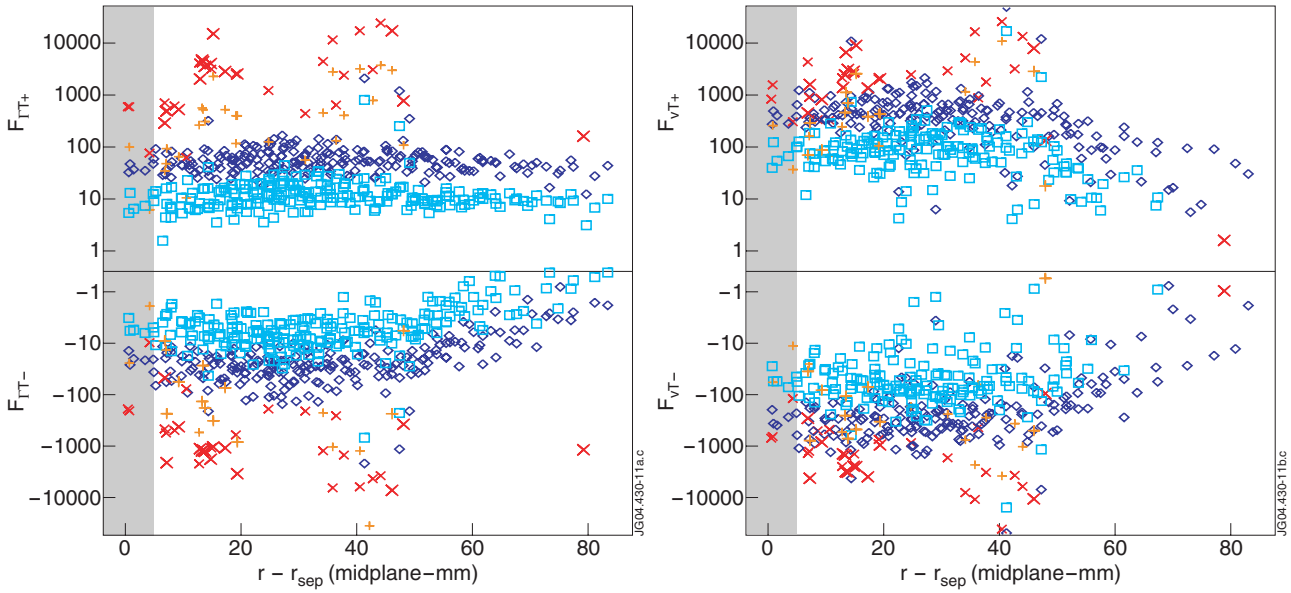

Figure 11: "Enhancement factors" $F_{\Gamma T\pm}$ (left) and $F_{vT\pm}$ (right) with T = 50, 500μs, as defined in eqs. (2)-(5). The symbols/colours are the same as in Fig. 10. The factors indicate how much larger the maximum values of turbulent radial particle flux Γ_r or effective radial velocity v_{reff}, averaged over 50μs or 500μs intervals, are as compared with averages over longer inter-ELM time intervals (2-20ms) at the same probe position.